Increasing Daytime Stability Enhances Downslope Moisture Transport in the Subcanopy of an Even-aged Conifer Forest in Western Oregon, USA

Stephen Drake[1], David Rupp[1], Christoph K Thomas[2], Holly Jayne Oldroyd[3], Mark Schulze[1], and Julia Allen Jones[1]

[1]Oregon State University
[2]University of Bayreuth
[3]University of California, Davis

November 22, 2022

Abstract

Mountain breezes including katabatic and anabatic flows and temperature inversions are common features of forested mountain landscapes. However, the effects of mountain breezes on moisture transport in forests and implications for regional climate change are not well understood. A detailed instrumental study conducted from July to September 2012 in an even-aged conifer forest in the Oregon Cascade Range was investigated to determine how temperature profiles within the forest canopy influenced atmospheric surface layer processes that ventilate the forest. Within-canopy inversion strength has a bi-modal relationship to sub-canopy wind speed and resulting moisture flux from the forest. On days with relatively modest heating of the top of the canopy and weak within-canopy inversions, above canopy winds more efficiently mix subcanopy air, leading to greater than average vertical moisture flux and weaker than average along-slope, sub-canopy water vapor advection. On days with strong heating of the top of the canopy and a strong within-canopy inversion, vertical moisture flux is suppressed, and daytime downslope winds are stronger than average under the canopy. Increased downslope winds lead to increased downslope transport of water vapor, carbon dioxide and other scalars under the canopy. Increasing summer vapor pressure deficit in the Pacific Northwest will enhance both processes: vertical moisture transport by mountain breezes when within-canopy inversions are weak, and downslope water vapor transport when within-canopy inversions are strong. These mountain breeze dynamics have implications for climate refugia in forested mountains, forest plantations, and other forested regions with similar canopy structure and regional atmospheric forcings.

Increasing Daytime Stability Enhances Downslope Moisture Transport in the Subcanopy of an Even-aged Conifer Forest in Western Oregon, USA

S. A. Drake[1,2], D. E. Rupp[2,3], C. K. Thomas[2,4], H. J. Oldroyd[5], M. Schulze[6], and J. A. Jones[2]

[1]Department of Physics, University of Nevada, Reno, Reno, Nevada, 89557, USA.

[2]College of Earth, Ocean, and Atmospheric Sciences, Oregon State University, Corvallis, Oregon, 97331, USA.

[3]Oregon Climate Change Research Institute, College of Earth, Ocean, and Atmospheric Sciences, Oregon State University, Corvallis, Oregon, 97331, USA.

[4]Micrometeorology, University of Bayreuth, Bayreuth, Germany.

[5]Department of Civil and Environmental Engineering, University of California, Davis, Davis, California, 95616, USA.

[6]College of Forestry, Oregon State University, Corvallis, Oregon, 97331, USA.

Corresponding author: Stephen Drake (stephendrake@unr.edu)

Key Points:

- Summer daytime forest canopy heating produces a within-canopy inversion and downslope flow isolated from above-canopy upslope airflow
- Increased canopy inversions enhance both subcanopy wind speed and downslope water vapor advection
- Regional climate change may increase moisture loss by subcanopy downslope advection and greater transpiration from even-aged conifer forests

Abstract

Mountain breezes including katabatic and anabatic flows and temperature inversions are common features of forested mountain landscapes. However, the effects of mountain breezes on moisture transport in forests and implications for regional climate change are not well understood. A detailed instrumental study conducted from July to September 2012 in an even-aged conifer forest in the Oregon Cascade Range was investigated to determine how temperature profiles within the forest canopy influenced atmospheric surface layer processes that ventilate the forest. Within-canopy inversion strength has a bi-modal relationship to sub-canopy wind speed and resulting moisture flux from the forest. On days with relatively modest heating of the top of the canopy and weak within-canopy inversions, above canopy winds more efficiently mix subcanopy air, leading to greater than average vertical moisture flux and weaker than average along-slope, sub-canopy water vapor advection. On days with strong heating of the top of the canopy and a strong within-canopy inversion, vertical moisture flux is suppressed, and daytime downslope winds are stronger than average under the canopy. Increased downslope winds lead to increased downslope transport of water vapor, carbon dioxide and other scalars under the canopy. Increasing summer vapor pressure deficit in the Pacific Northwest will enhance both processes: vertical moisture transport by mountain breezes when within-canopy inversions are weak, and downslope water vapor transport when within-canopy inversions are strong. These mountain breeze dynamics have implications for climate refugia in forested mountains, forest plantations, and other forested regions with similar canopy structure and regional atmospheric forcings.

Plain Language Summary

The summer and fall seasons in the Pacific Northwest are typically warm and dry, and solar radiation and locally generated breezes affect temperature and moisture of air in the forest canopy. In forest plantations, which have uniform height, canopy heating creates an inversion – an increase of temperature with height under the forest canopy. On days with strong canopy heating, this inversion limits moisture loss through the top of the canopy and enhances winds that flow downslope below the canopy, carrying moisture out of the system. On days with less canopy heating, winds mix air above and within the canopy and promote moisture loss to the air above the forest canopy. Regional models of future climate simulate declining dry-season relative humidity. Collectively, these findings indicate that future climate will enhance both vertical and downslope moisture loss during the dry season from forest plantations, which represent a large fraction of forest cover of the Pacific Northwest of the US.

1 Introduction

An increasing fraction of global forest area consists of plantation forests (Hansen et al., 2013). Plantations typically are even-aged, with a single species and simple canopy structure (Lefsky et al., 1999). Past management practices have led to millions of acres of dense, uniform stands on federal forests and private land in the Pacific Northwest (PNW) where conifer forests are the predominant land-cover in mountainous terrain. Several recent studies have reported that even-aged conifer forests evapotranspire more water than reference, native, multi-storied forests during the dry summers in the Pacific Northwest and British Columbia, Canada (Perry & Jones, 2017; Gronsdahl et al., 2019; Segura et al., 2020), with potential implications for regional water supply (Jones & Hammond, 2020). Yet despite the important role of forest plantations in mediating land cover responses to climate change, the effects of forest plantation canopy structure on atmospheric flows of heat and moisture are not well understood.

Forest canopy structure affects through-canopy mixing and therefore sensible heat and moisture fluxes (Freundorfer et al., 2019; Thomas et al., 2013). Studies have shown that maximum air temperature and vapor pressure deficit are lower under forest canopies than nearby unforested areas (Karlsson, 2000; Ferrez et al., 2011). The forest water balance plays a key role in buffering forest response to warming and increased vapor pressure deficit (Davis et al., 2019). Regional climate processes and local terrain produce areas of relatively cool temperature in forested mountains, which have been described as "microrefugia" (Dobrowski et al., 2011; Lenoir et al., 2017). Many recent studies have attempted to model sub-canopy temperature (e.g., Holden et al., 2016; Lembrechts and Lenoir, 2020). Yet observational studies of heat and moisture transfer in forest canopies are lacking (de Frenne et al., 2021; Thomas, 2011). A better understanding of sub-canopy heat and moisture transport is relevant to topics as diverse as cold air pooling, moisture transport and losses, and wildfires (Richie et al., 2007; Daly et al., 2010; Frey et al., 2016; Davis et al., 2017).

Temperature inversions are frequent in forested mountains, even during daytime in summer (Daly et al., 2010, Minder et al., 2010, Rupp et al., 2020). Landscape-scale inversions and cold air pooling result from differential landscape heating (e.g., Lundquist & Pepin, 2008). In addition, heating of the forest canopy influences temperature gradients and moisture exchange (Brutsaert & Parlange, 1992; Leuzinger & Körner, 2007), and contributes to the formation of an inversion within the canopy, especially under the uniform canopy structure of a plantation forest (Hosker et al., 1974). Within-canopy inversions modulate the influence of above canopy winds on the sub-canopy by limiting vertical mixing into the sub-canopy (Launiainen et al., 2007; Thomas and Foken, 2007). Within-canopy inversions tend to weaken during the night (Whiteman, 1982; Juang et al., 2006) and re-establish and strengthen during the day (Raynor, 1971; Staebler et al., 2005; Froelich and Schmid, 2006; Tóta et al., 2012). Although models have explored how forest canopy structure influences air flows in mountain valleys (Kiefer & Zhong, 2013, 2015), few studies have examined the interaction between within canopy temperature inversions and airflow within forest canopies in mountain landscapes.

The objective of this study is to determine how summertime heating of the canopy of a dense plantation forest influences movement of heat and moisture into, out of, and within the forest canopy in a steep mountain watershed, which is typical of much of the Pacific Northwest of the US. The study quantified sub-canopy atmospheric processes in a 45-yr-old plantation forest characterized by a uniform single-layer canopy during the summer dry season when plants are drought stressed and therefore more sensitive to subtle environmental changes (Hughes, 2000). Subcanopy flow regimes are then examined in the context of regional climate change predictions over PNW forests to investigate the feedback between canopy heating and subcanopy moisture transport.

2 Materials and Methods

2.1 Study site

The study was conducted from July through September of 2012 in a sub-basin of Lookout Creek (64 km^2), in the HJ Andrews Experimental Forest (HJ Andrews) and Long-Term Ecological Research (LTER) site in the central western Cascades of Oregon, USA (122.25° W, 44.21° N). Slope gradients range from 30 to more than 60% in the HJ Andrews, and steep tributary valleys, such as the study site, drain to a central valley. Mean annual temperature is 9.7 °C and mean annual precipitation is 2350 mm. Less than 5% of precipitation occurs during the dry season (July 1 – September 30) (Harr, 1983). The study site was Watershed 1 (WS1, Figure 1), a relatively small (96 ha), steep (average slope ~60%) northwest facing valley near the outlet of Lookout Creek Basin. Elevation ranges from 460 to 990 m in WS1, and from 430 to >1600 m in Lookout Creek. The original vegetation of WS1, old growth Douglas-fir (*Pseudotsuga menziesii*) (150 to 500-yrs), was clearcut and cable yarded between 1962 and 1966, and the remaining slash was subsequently broadcast burned in 1966 (Fredricksen, 1970; Perry & Jones, 2017) (Figure 2). Douglas-fir was planted and aerially seeded during the late 1960s. As of 2012, the planted forest consisted of a dense stand of ~45-yr-old Douglas-fir with deciduous red alder (*Alnus rubra*) along the stream channel (Figure 2). The average height of the canopy was 29 m, and the canopy extended down to 8 m above the ground, with understory vegetation from 1 to 4 m high. Many studies in WS1 have examined post-disturbance succession, ecohydrology, and carbon budgets, and other topics (e.g.: Halpern et al., 1990; Hicks et al., 1991; Moore et al., 2004; Pypker et al., 2007; Hood et al., 2006; Argerich et al., 2016). Basal area, growth rates, and density in the forest plantation in WS1 are within reported ranges for managed and unmanaged forest plantations on steep watersheds in western Oregon (Perry & Jones, 2017).

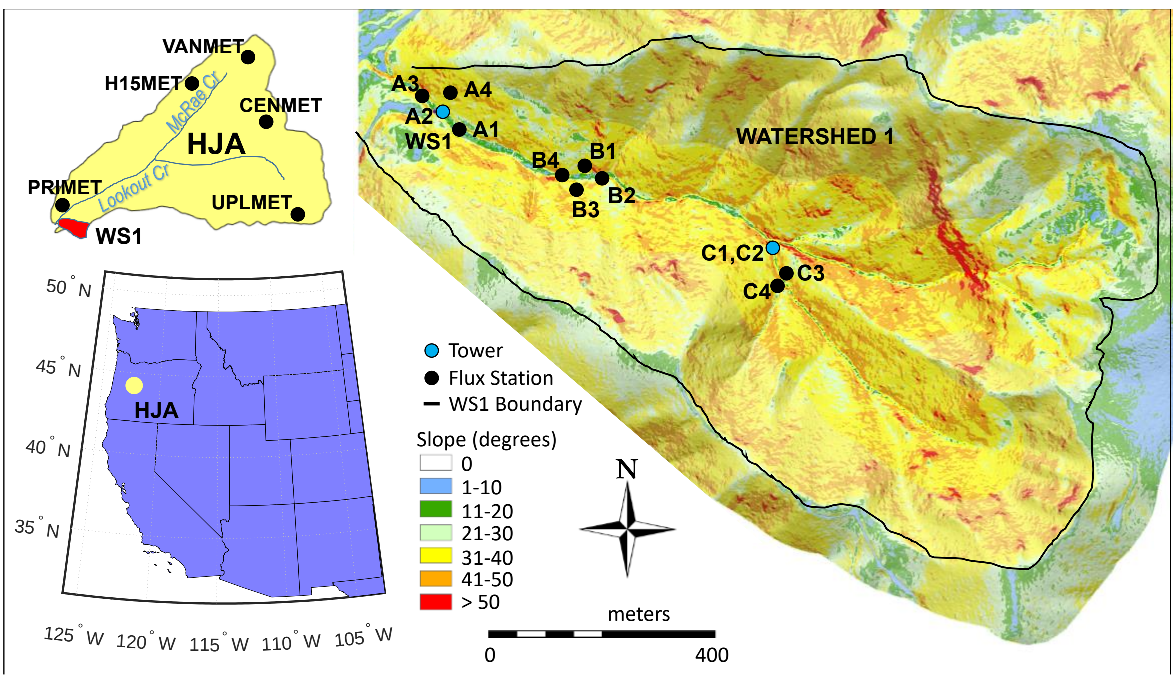

Figure 1. Overview maps show the location of the HJ Andrews Experimental Forest in Oregon, the locations of benchmark stations and the WS1 tower within the HJ Andrews domain and flux

station locations within Watershed 1. (source: Theresa Valentine, Corvallis Forest Science Laboratory). The Watershed 1 stream drains into Lookout Creek 150 m below station A3.

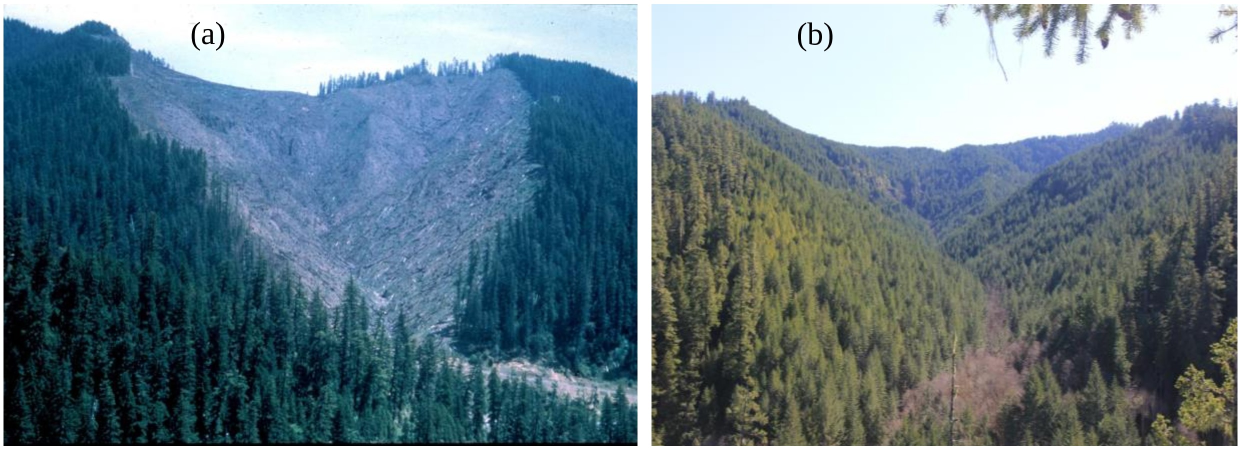

Figure 2. Watershed 1 viewed from the north after clear-cut in the late 1960s (panel a, Photo: Dick Fredricksen) and in 2019 (panel b, Photo: Mark Schulze).

2.2 Data collection

Air flow, heat, and moisture were measured within three sub-domains along the valley axis (Figure 1). Enclosure-mounted data loggers (Model CR3000, Campbell Scientific Inc. Logan, UT, USA) were deployed at three base sites ranging from 470 m to 580 m elevation along a ~1-km transect up the WS1 valley floor from Lookout Creek. At each base site, designated as “A”, “B”, and “C,” data were collected from four stations, labeled e.g., A1, A2, A3 and A4, etc. Stations were positioned with the primary goal of measuring sub-canopy wind, temperature, and moisture along the valley axis (stations A1, A2, A3, B2, B4, C1, C2, C4) and with secondary goals of resolving winds in open locations (station A4) and drainage flow contributions from side slopes (B1, B3) and tributary channels (C3, Figure 1). Sensors were mounted on tripods at 2 m nominal height above ground level (agl) and aligned with local gravity. Sensors at sites A2, C1, and C2, were positioned higher above ground to further resolve bole-space characteristics. Here, “bole-space” is taken as the air volume between the lower fringe of the canopy and the ground. Sensors at A2 were mounted at the 16-m level of a 37-m tower designated as WS1 Tower (Figure 1). Sensors at C1 and C2 were mounted at 7.4 m and 12.9 m (boom-extended) on a 12.2-m tower. All A, B and C sensors were placed within or below the canopy, except station A4, which was located in a SW-facing canopy opening on a slope 120 m uphill from the WS1 tower (Figure 3a).

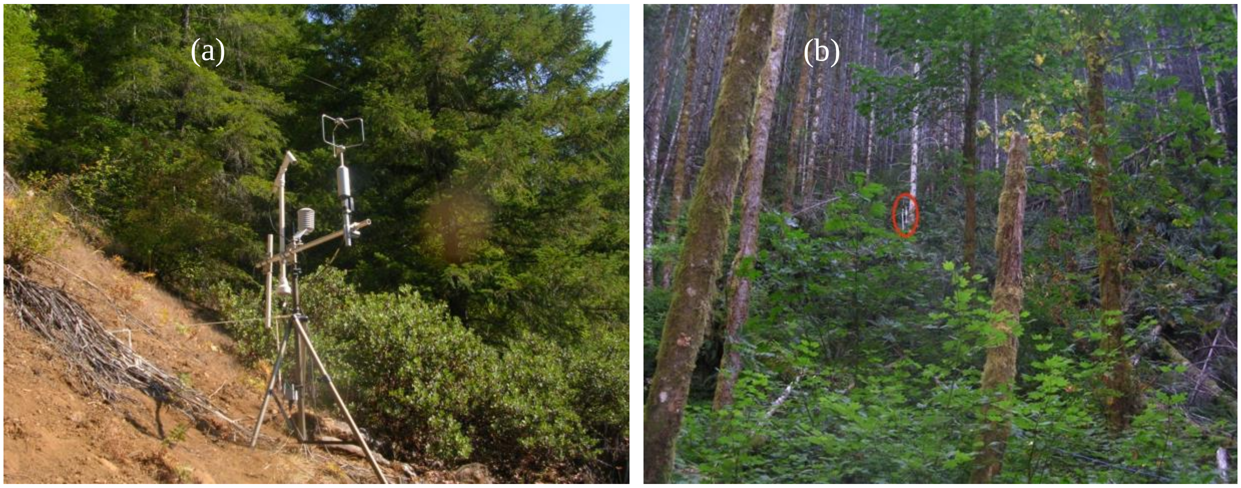

Figure 3. Photographs of example stations. (a) Station A4 was located in a SW-facing canopy opening on a slope 120 m uphill from the WS1 tower. (b) Station B3 was located on a forested slope and identified by a red ellipse. (Photo: Stephen Drake).

Wind speed and direction were sampled at 20 Hz using ultrasonic anemometers (Model Young VRE81000, RM Young, Traverse City, MI, USA), hereafter referred to as “sonics”. One-minute averaged temperature and humidity were measured using aspirated thermohygrometers (Model Vaisala HMP 155, Vaisala, Finland) paired with each sonic. Thermohygrometers were mounted in actively aspirated radiation shields (Thomas & Smoot, 2013) with inflow at centroid height of the sonic volume.

Additional sensors were mounted on the 37-m WS1 tower in order to determine within-canopy stability and to measure above canopy winds near the watershed outlet. The WS1 tower extended 4 m above the top of the canopy (33 m). Temperature was measured using aspirated thermistors (Model 107, Campbell Sci., Logan, UT, USA) mounted at 1, 7, 12, 18, 23, 29 and 37 m and recorded at 1-minute averages by a datalogger (Model CR23x, Campbell Scientific, Logan, UT, USA). Tower-mounted instrumentation used in this investigation included open-path CO_2/H_2O analyzers (Model Licor LI-7500, Licor, Lincoln, NE, USA) at 4 and 37 m, an additional sonic anemometer at 4 m (Model CSAT3, Campbell Scientific, Logan, UT, USA), and a 3-axis sonic anemometer at 37 m (Model Gill R2, Gill Instruments, Lymigton, UK) sampled at 20 Hz and recorded by a datalogger (Model CR3000, Campbell Scientific Ltd. Logan, UT, USA).

Wind speed and direction, air temperature and moisture data obtained in the WS1 watershed were averaged to 1-minute intervals.

2.3 Basin-scale and regional reanalysis data

Basin-scale (Lookout Creek) data of wind speed and direction for the study period were obtained from five HJ Andrews benchmark stations: PRIMET (436m), H15MET (909m), CENMET (1028 m), VANMET (1268 m) and UPLMET (1298 m) (Figure 1). Wind speed and direction are measured at 10 m (except for H15MET which was at 5 m) using propeller anemometers (Model, 05103 Wind Monitor, RM Young, Traverse City, MI, USA). Data were averaged to 15-minute intervals. The propeller on this anemometer has a 1 m s^{-1} minimum threshold (Campbell Scientific, 2015). Sub-1 m s^{-1} averages were kept in subsequent analyses to resolve the diurnal cycle of wind speed with the potential that sub-1 m s^{-1} measurements that constitute the 15-minute averages may have systematically skewed 15-min wind averages downward during periods with weak winds. The impact of this potential systematic error was minimized by comparing relative changes in wind speed rather than absolute wind speed. Benchmark stations are located in canopy gaps, and the sensor heights are below the surrounding forest canopy, which decreased measured wind speed.

Regional-scale wind data for the study period were obtained from the land component European Centre for Medium-Range Weather Forecasts (ECMWF) Re-Analysis 5 (Muñoz-Sabater et al., 2021; Hersbach et al., 2020). This product combines observations and model physics to reproduce hourly atmospheric state variables and derivatives with land surface variables interpolated to grid points with 0.1° × 0.1° resolution.

Spatially distributed and synchronous measurements of temperature, wind speed, barometric pressure, and humidity were available for 50 of the 55 days between July 25 and Sept 17 for which. Data gaps occurred for three days with the 1 m temperature sensor and for two days with the 4 m sonic anemometer on the WS1 tower. Hereafter, these 50 days are referred to as the 50-day IOP (Intensive Observation Period).

2.4. Data analysis

To identify the persistence and timing of wind patterns, diel airflow measurements at the WS1 tower were composited (averaged) to highlight features that are commonly observed during the same time daily. Before compositing potential temperature profiles, observed dry-bulb air temperature was converted to potential temperature by correcting for the dry-adiabatic lapse rate of 9.8 K km^{-1}, accounting for temperature differences due to elevation. Individual daily plots were compared with composites to verify that a single, large amplitude anomalous feature on a given day did not unduly bias time composites. Daily composite data were divided into four distinct time periods based on wind speed and direction following Whiteman (1990) and Pypker et al. (2007). The four time periods are: daytime flow (DF), evening transition (ET), nighttime conditions (NC) and morning transition (MT). During clear-sky conditions, the DF time period is distinguished by thermally-driven upslope flow above the canopy. The ET time period begins when above-canopy wind direction reverses and air flows downslope. The NC time period begins as turbulence weakens, and NC transitions to the MT as insolation initiates upslope flow above the canopy the following morning.

The strength and effects of the within-canopy inversions created by heating of the forest canopy were examined by calculating static stability, wind speed, and latent heat flux during daytime flow (DF) at the WS1 tower for the 50-day IOP. Maximum sub-canopy static stability (Stull, 2012) was computed during the time period of peak canopy heating (13:30 to 14:30, local time). Static stability was computed as the average potential temperature difference between the 1 and 23 m heights on the WS1 tower divided by the difference in height (K m^{-1}). Static stability is used as a measure of sub-canopy stability rather than the stability parameter used in Wang et al. (2015) because the Obukhov length is not a valid stability parameter within the roughness sublayer (Vickers & Thomas, 2014), or for katabatic flow (Oldroyd et al., 2016). Bole-space wind speed and direction were calculated at 4 m height on the WS1 tower for the same 13:30 to

14:30 time frame as static stability. Wind direction was classified into two categories: variable (all directions) and down-valley, defined as wind direction ±25° within the most prominent down-valley direction. During periods of variable winds, even if the wind has a down-valley component, intermittent turbulence and coherent structures in above canopy winds may have significantly influenced the sub-canopy wind direction during discrete events. These one-hour averages of static stability, wind speed and wind direction variability were used to characterize wind regimes as a function of subcanopy static stability.

Turbulence kinetic energy (TKE) is the kinetic energy, usually expressed per unit mass, associated with eddies in a turbulent flow. TKE in the sub-canopy drives the vertical exchange of moisture across the boundary from the forest canopy to the air above. Thirty-minute averaged turbulence kinetic energy (TKE) was calculated for each station as (Stull, 2012):

$$\frac{TKE}{m} = 0.5\left(\overline{u'^2} + \overline{v'^2} + \overline{w'^2}\right) \quad , \qquad Eq\ (1)$$

where m is mass, u', v', and w' are instantaneous deviations from 30-minute mean wind components and the overbar represents a 30-minute average. TKE was calculated for subcanopy stations at the 2-m nominal height of the sonic anemometers.

Turbulence intensity (TI) is defined as the standard deviation of wind speed, σ_M, divided by the mean wind speed, $\overline{M}$, (Stull, 2012):

$$TI = \frac{\sigma_M}{\overline{M}} \ . \qquad Eq\ (2)$$

and provides a normalized measure of turbulence.

To assess the relationship of within-canopy dynamics in Watershed 1 to the basin and the region, data on wind speed from benchmark stations PRIMET (430m elevation), H15MET (909m), CENMET (1020m), VANMET (1275m), and UPLMET (1295m) throughout HJ Andrews (Figure 1) were averaged for each day of the study period.

To assess the effect of within-canopy inversions and winds on moisture fluxes within and through the forest canopy, the difference in water vapor concentration in the sub-canopy compared with the air above the canopy was determined as water vapor concentration (mol m^{-3}) at 4 m minus the water vapor concentration at 37 m, integrated over the daytime flow period, for each day of the study period, and this was related to the maximum static stability on each day.

To test the hypothetical effect of climate warming on sub-canopy winds and moisture transport, we calculated wind speed and virtual temperature differences between stations B4 and C4 along the main channel for days with relatively high in-canopy stability and determined the relationship between these air temperature and wind speed differences between these two sites. We then used this relationship to determine the effect of a 0.1 K m^{-1} increase in static stability on downslope water vapor transport by subcanopy winds. As in prior studies from this site (i.e., Pypker et al., 2007), downslope moisture transport is computed at the airshed exit although localized moisture fluxes are also present within the watershed boundary where moisture gradients are present.

3 Results

Above and sub-canopy wind speed and direction are composited for the experimental period in Sections 3.1 and 3.2 to summarize the local wind patterns. Winds are then categorized into four daily time periods (Section 3.3). We examine how inversion strength (static stability) is related to wind speed and how turbulence and latent heat flux varies over the day, above and below the canopy, for low-stability and high-stability conditions (Section 3.4). We show that on days with high static stability, the downslope subcanopy wind speed increases with stability, and low-stability days are associated with higher turbulence intensity but lower temperature below the canopy (Section 3.5). The coherence of sub-canopy wind and above-canopy winds within the larger Lookout Creek basin are investigated in Section 3.6. In Section 3.7 results indicate that stronger within-canopy inversions are associated with greater sub-canopy humidity, relative to the air above the canopy, and these stronger within-canopy inversions (on high-stability days) constrain within-canopy mixing and vertical moisture flux out of the canopy relative to low-stability days. Finally, we use the relationship of wind speed and virtual temperature differences between stations B4 and C4 along the main channel for high-stability days to test the hypothetical effect of warming on sub-canopy winds and moisture transport (Section 3.8).

Summer and fall seasons in the PNW are typically dry, dominated by a persistent high pressure synoptic pattern. However, June 2012 antecedent conditions in the HJ Andrews region were very moist with a Palmer Z index between 2.5 and 3.5 (NOAA NCDC Annual Drought Report, 2012, see also supplement section S1). During the study period (July 19, 2012 to September 17, 2012), Oregon ranked as the 2nd driest state and much of the continental US experienced drought conditions throughout this time period. Consequently, the progressive decrease in latent heat flux between the beginning of July and end of September was representative for a drought index transition from very moist to severe drought conditions. The prolonged dry period during the study period provided favorable conditions for isolating the effects of within-canopy stability on sub-canopy moisture transport.

3.1 Above vs. below-canopy winds

Based on 1-minute averaged data acquired from July 25 to Sept 17, 2012, wind above the canopy at WS1 tower had two prominent directions: from the NW and from the ENE (Figure 4a). The strongest winds were from the NW due predominantly to up-valley daytime flow and topographic steering rather than synoptic forcing at this locale (see also Figure S2 with overview of synoptic forcing in the supplement). Above the canopy, weaker down-valley (Lookout Basin) and down-slope winds from the eastern portion of the Watershed 1 basin were common during nighttime throughout the study. Wind above the canopy was more variable than below the canopy, in part due to 3-dimensional vorticity of turbulent eddies at the time scale of 1-minute averages. In contrast, wind direction below the canopy at 4-m height was bimodal, aligning with the watershed axis (Figure 4b). Sub-canopy wind direction along the valley axis was primarily down-valley throughout the day (Figure 4b). The consistently lower speed and more directional winds at 4 m compared to 37 m indicate that the canopy acts as a permeable mechanical and thermodynamic barrier that dampens through-canopy turbulent fluxes.

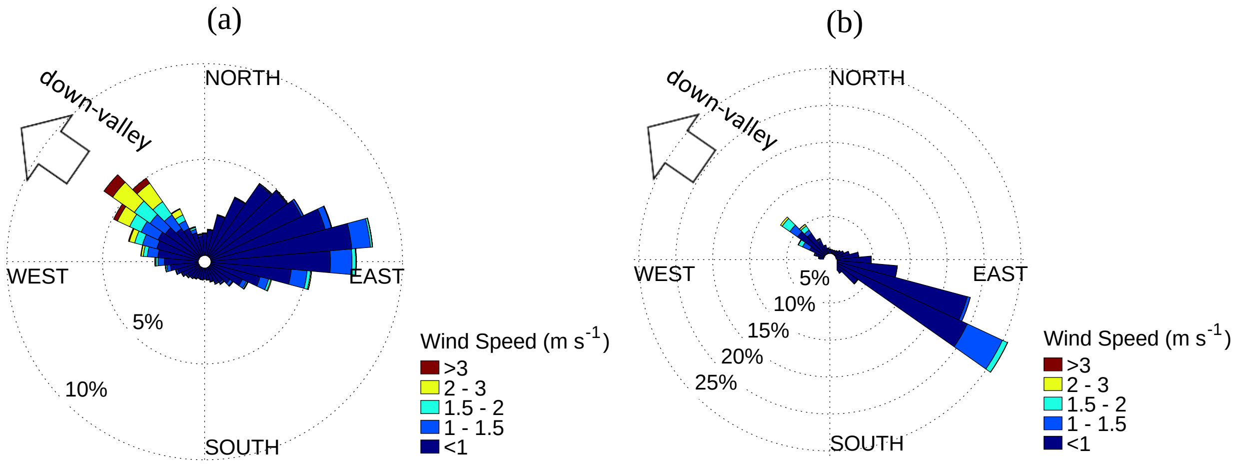

Figure 4. Windroses on WS1 tower color-coded by wind speed at 37 m AGL (above canopy, panel a) and at 4 m AGL (below canopy, panel b).

3.2. Wind patterns as a function of canopy cover and position within the watershed

Below the canopy (2 m), downslope winds occurred throughout the watershed during both daytime and nighttime. The relative frequency of downslope flow varied by position in the watershed and by canopy cover (Figure 5). Below-canopy winds were primarily downvalley throughout the day at sites located along the axes of tributaries in the upper valley (C2, C3, C4) and at sites aligned with the channel axis in the mid-valley (B2 and B4). In contrast, below-canopy wind direction was primarily downslope at sites positioned slightly higher above the valley axis (B1 and B3); these sites were dominated by downslope rather than down-valley flow because they were positioned generally above the depth of down-valley cold air drainage flows. In addition, wind direction was quite variable at a location having a canopy opening (site A4, Figures 3a and 5); this site was exposed to above-canopy winds, multi-scale forcing, edge effects and turbulence, which disrupt the nocturnal/downslope, daytime/upslope wind regime.

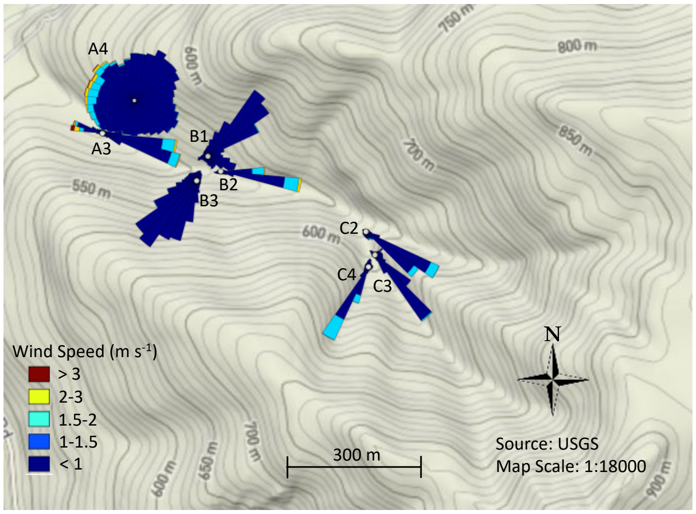

Figure 5. Windroses of 1-minute averaged winds at 2 m nominal height for subcanopy stations A3, A4, B1, B2, B3, C2, C3 and C4 in Watershed 1. Stations A1 and B4 have very similar windrose shapes as station A3 in Figure 5 but are not rendered to avoid overlapping. Windrose bin sizes are rescaled to avoid overlap and highlight features described in the text. (Map source USGS)

3.3 Four time periods of wind

Average wind speed and direction at the WS1 tower clearly display four time periods of: morning transition, daytime flow, evening transition, and nighttime conditions (Figure 6a). After the morning transition (MT), wind speed above and below the canopy increases during the daytime flow period and gradually diminishes throughout the nighttime conditions period (Figure 6a). During the morning transition, solar heating in Lookout Creek Basin erodes the cold air pool and sub-canopy gravity-driven flow increases following a brief, weak wind direction reversal (Figure 6b). This sub-canopy MT wind reversal is likely caused by a pressure gradient adjustment during the transition from the nighttime conditions to daytime flow (NC to DF) period and is characteristic of transition periods in mountainous regions (Nadeau et al. 2012; Nadeau et al. 2018). Above the canopy, downslope winds exhibit a local maximum in magnitude during MT (Figure 6a), as solar heating in Lookout Creek Basin initiates a mountain breeze that precedes solar heating in the Watershed 1 basin (see also Section 3.6).

The maximum inversion (5.6 °C difference in temperature at 37 m vs. 1 m) occurred at 14:46, consistent with canopy heating by solar insolation (Figure 6c). During the daytime flow (DT), the sub-canopy wind speed peaks at 14:36, about 10 minutes before the time of maximum temperature inversion within the canopy, whereas the above-canopy wind speed peaks at 15:15, about 29 minutes after the time of maximum inversion (Figures 6a, 6c). During the evening transition (ET), wind directions roughly align above and below the canopy as nocturnal drainage flow reestablishes above the canopy. Gravity flow decreases throughout the night, as nocturnal drainage flow fills the valley with cold air, until the morning transition and the diurnal cycle repeats.

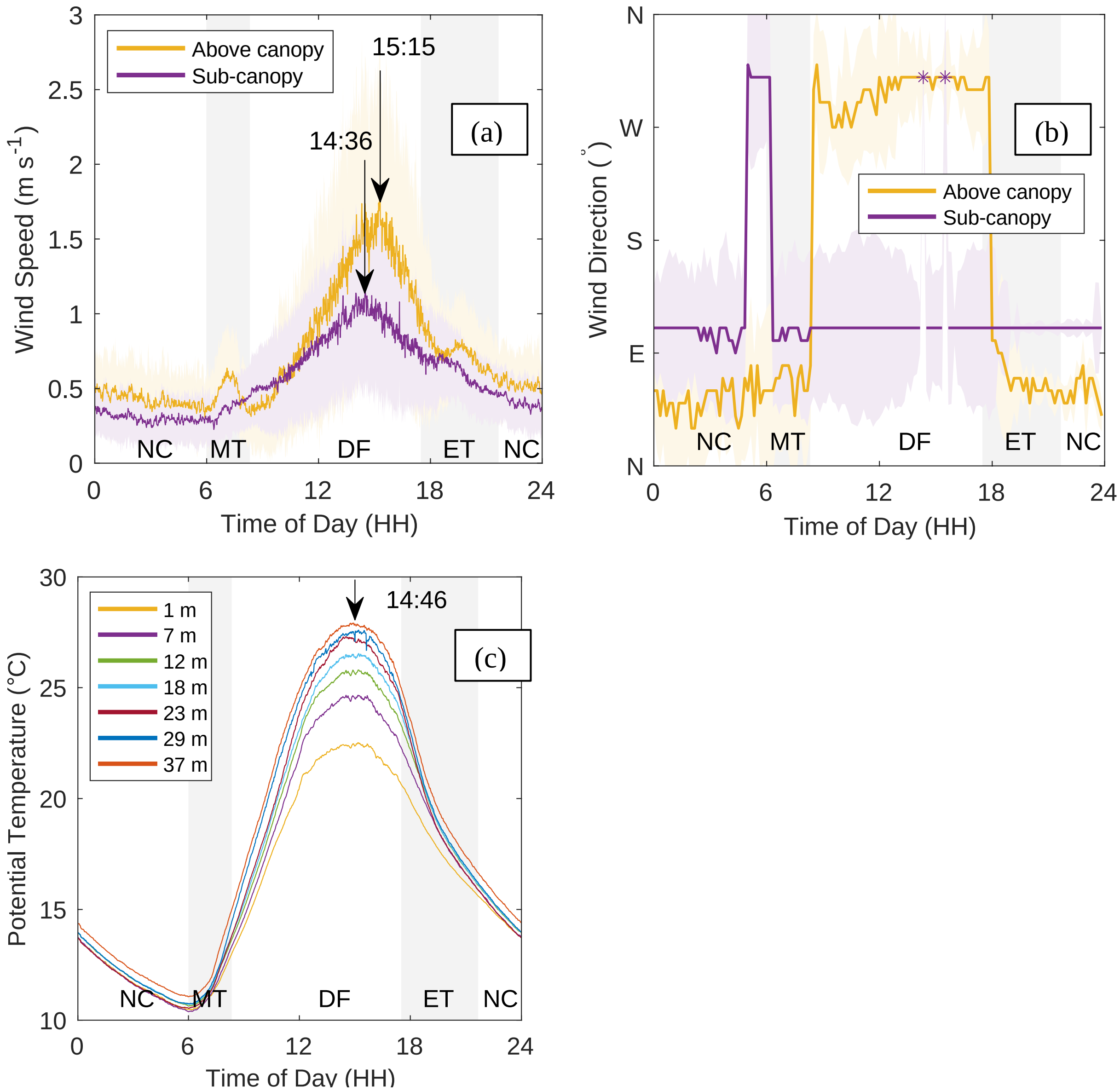

Figure 6. Composite wind speed (a), wind direction (b) and potential temperature for heights ranging from 1 to 37 m (c) at the WS 1 tower for the period July 19, 2012 to Sept. 17, 2012, and four flow regimes (vertical white and grey bars): daytime flow (DF), evening transition (ET), nighttime conditions (NC) and morning transition (MT). Flow regimes are defined as in Whiteman (1990) and Pypker et al. (2007). Wind speed is shown above the canopy at 37 m (gold) and below the canopy 4 m (purple) (panel a) with time of peak winds delineated by arrows. Composite wind directions are defined by the mode of wind direction at each minute in 10-degree bins (panel b). Shading indicates one standard deviation. Purple asterisks in panel (b) indicate two short time periods when the subcanopy wind direction mode at the WS1 tower was preferentially upvalley.

The sub-canopy diurnal wind direction response in the WS1 basin (Figures 5 and 6) is different from the archetypal mountain breeze regime. An archetypal, thermally-driven mountain breeze presents upslope flow during the DF period that increases with increased heating (Schmidli, 2013). In contrast, along the valley axis the dominant subcanopy wind direction was down-valley (Figure 5), and the highest sub-canopy wind speeds were downvalley at representative stations along the valley axis (Figure 6a, 6b). These differences appear to be due to the presence of an even-aged dense forest canopy, which creates an inversion that modulates below-canopy air flows.

3.4 Daytime flow mode

Over the 50-day IOP the relationship of 4 m sub-canopy wind speed to static stability differs below and above a stability transition zone (grey bar in Figure 7a). For days with static stability values below 0.17 K m^{-1}, wind speed is not correlated with stability (red data points, R^2=0.04). For days with static stability values above 0.21 K m^{-1}, down-valley wind speed increases with increasing static stability (blue data points, R^2=0.42). Other factors, such as the coherence of diel pressure gradient evolution and shortwave solar insolation also influence wind speed (Figures S3 and S4 in the supplement).

The standard deviation of vertical wind speed, σ_w, was greater during low stability compared with high stability days, both above and below the canopy (Figure 7b), indicating greater potential for vertical mixing on low-stability days. The standard deviation of vertical wind speed was many times higher above than below the top of the canopy (Figure 7b). Below the canopy, the low stability maximum σ_w (~0.1) was twice the high stability value (~0.05), while above the canopy, the low stability maximum σ_w (0.33) was 33% greater than the high stability value (0.25). These findings, combined with the relationship of wind speed to stability (Figure 7a), indicate that within-canopy mixing was suppressed on high-stability days relative to low-stability days. The likely physical mechanism for this σ_w reduction is the enhanced temperature inversion on high stability days, because the buoyancy restoration force has larger magnitudes in stably stratified fluids (Vickers & Thomas, 2013).

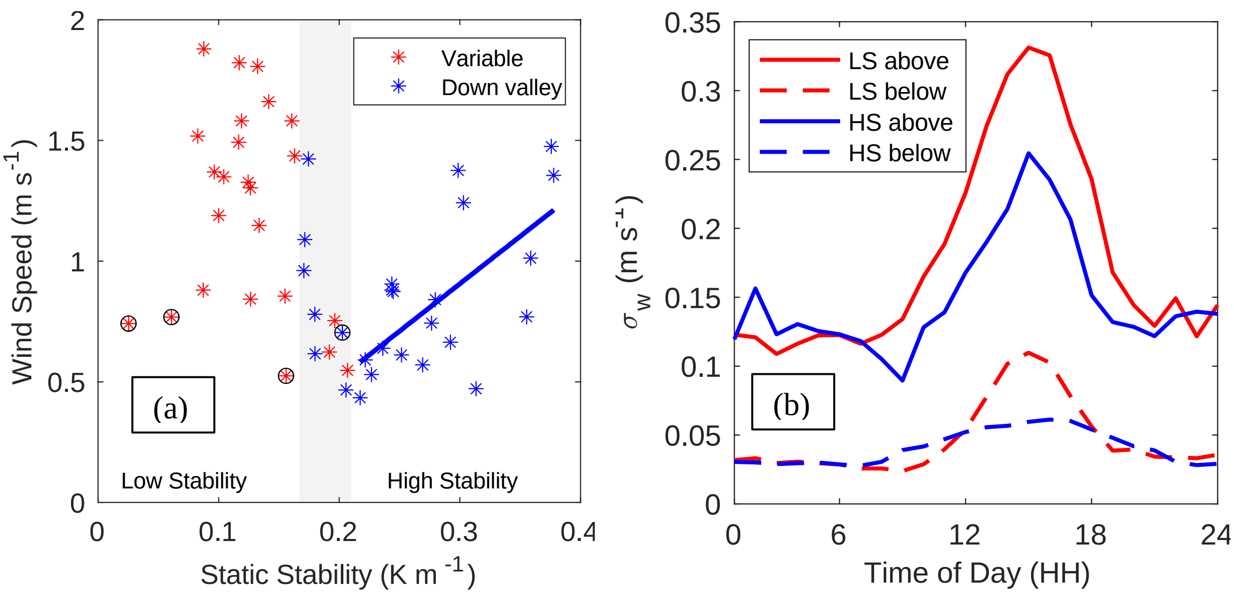

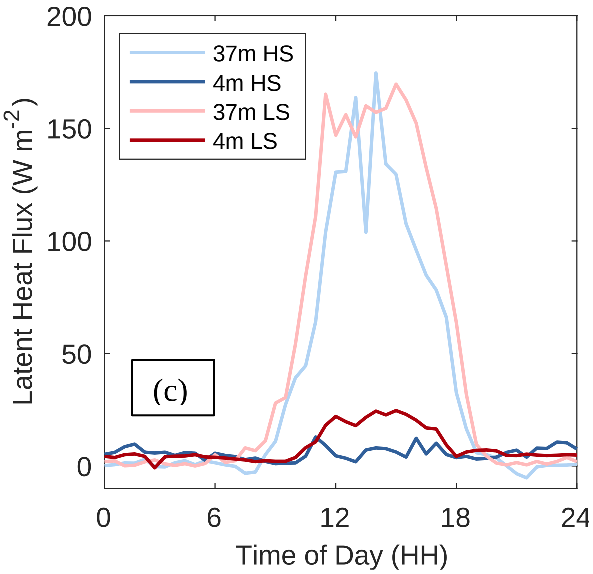

Figure 7. Relationship of composite 4 m wind speed to static stability (a); composite σ_w over the day (b); and composite latent heat flux over the day (c). Panel (a) shows WS1 tower 4-m mean wind speed vs. canopy static stability over the 1 to 23-m layer during the time period 13:30 to 14:30 for each of the 50-day IOP. Wind speed is coded by dominant daily wind direction (variable = red, or downvalley= blue). Overcast days are circled. (b) Composite standard deviation of the vertical wind speed component by time of day computed at 37 m (above canopy) and 4 m (below canopy) heights for low static stability (LS) and high static stability (HS) days indicated in panel (a). (c) Composite latent heat flux at 4-m and 37 m heights for LS and HS days.

These effects on vertical mixing produce much higher latent heat fluxes just above the canopy compared to within the canopy, and 26% greater vertical moisture loss via mixing during low-stability compared to high-stability days just above the canopy (37 m) (Figure 7c). But for brief spikes at 13:00 to 15:00 on high-stability days, latent heat fluxes at 37 m were higher throughout the DF period during low-stability days compared with high-stability days, indicating more continuous through-canopy mixing on low-stability compared with high-stability days.

The finding of distinctly different DF flow regimes permit classifying days in the 50-day IOP according to their daytime flow values of static stability and associated moisture flux characteristics (Figure 8). Twenty-one of the 50 days were low-stability, 19 were characterized as high-stability and 10 days were transitional. Low- and high-stability periods tend to persist for several consecutive days.

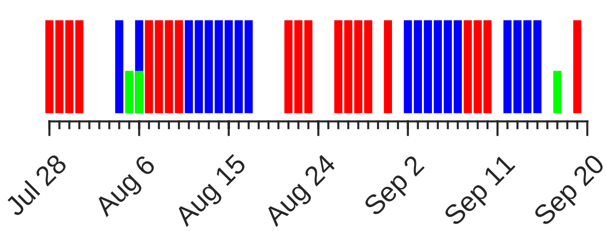

Figure 8. Days in the 50-day IOP classified as low-stability (red) or high-stability (blue), based on analysis in Figure 7a. Days with precipitation are shown in green.

Atmospheric conditions that differentiate low-stability from high-stability days are examined in the supplement. A distinguishing characteristic of HS days is synchronicity of the pressure tendency that is lacking on LS days. As will be shown in Section 3.6, the basin-wide, daytime change in wind speed is smaller on HS days relative to LS days.

3.5 Along-valley wind characteristics

Subcanopy wind speed during daylight hours in the July 25 to Sept 17 study period was consistently higher on high-stability days than on low-stability days at the three stations along the Watershed 1 valley axis (A1, B4, C4) (Figure 9a). Wind speed also was more variable during LS days (shades of red in Figure 9a) than HS days. Composite virtual temperature (T_v) was also greater on HS compared with LS days at stations A1, B4 and C4 (Figure 9b). Lower sub-canopy T_v during LS days compared with HS days may be the result of a weaker inversion and greater prevalence of large, coherent eddies on LS days that inject relatively dry above-canopy air into the sub-canopy. Several overcast days (Figure 7a, Figure S4) also contributed to lower ensemble sub-canopy T_v during LS days.

During the afternoon on HS days, air at station C4 (an upstream tributary) was denser (had a lower T_v) than at B4 or A1 (in the main channel) (Figure 9b). Denser air increased katabatic acceleration at C4 relative to B4 or A1, producing the higher wind speed observed at C4 compared with A1 or B4 (Figure 9a). Even for LS days, a katabatic signature was evident at station C4 where increased afternoon cooling relative to stations A1 and B4 was associated with an increase in afternoon wind speed (Figures 9a, 9b). On the other hand, on HS days T_v and wind speed at midday were higher at B4 (axis of main channel, midway down the valley) than A1 (axis of main channel, near mouth of the watershed), counter to the density effect on katabatic acceleration. This discrepancy could be attributed to mass continuity and the widening of the valley floor at A1, which increases sub-canopy volume thereby slowing sub-canopy winds. Differences in subcanopy roughness and canopy elements between stations also may be a contributing factor in the observed differences in subcanopy wind speed (Thomas, 2011), despite efforts to locate stations to minimize along-slope flow disruption by vegetation.

Turbulence kinetic energy was higher during daylight hours, higher on low-stability compared to high-stability days, and higher at stations A1 (valley mouth) and C4 (upper valley) than B4 (midway down the valley) (Figure 9c). Station B4 had relatively low TKE on both LS and HS days whereas station A1 exhibited the highest TKE for all days. As before, high variability in wind speed and enhanced TKE generation can be attributed to proximity of station A1 to the WS1 airshed outlet to Lookout Creek. Relatively low subcanopy wind speeds (Figure 9a) coincided with relatively high TKE on LS days at A1, and the highest average composite wind speed coincided with the lowest average composited TKE at 1500-1800h on HS days at station C4 (Figure 9c). While increased wind speeds, which at these subcanopy sites occur with the HS condition, are typically related to high shear generation, higher stability likely suppresses vertical TKE transport across the canopy. This result is consistent with Figure 7b, which showed that on LS days above canopy winds ventilate the subcanopy and large eddies introduce TKE into the subcanopy environment. Below the canopy, vertical mixing is enhanced along the valley axis on LS days and suppressed on HS days.

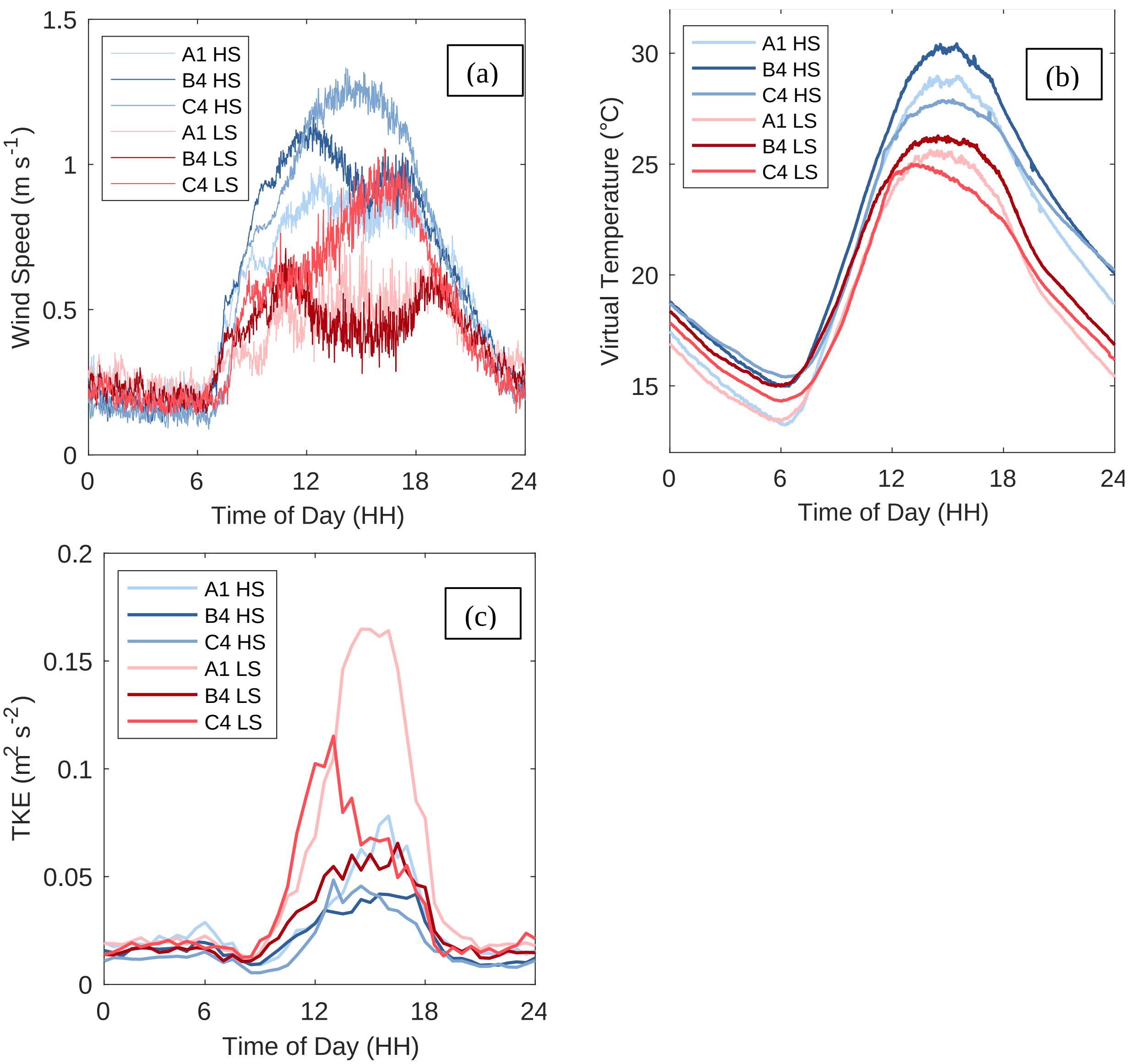

Figure 9. Comparing sub-canopy wind speed during HS and LS days at selected stations in WS1 (panel a). In panel (b), sub-canopy 1-minute averaged virtual temperatures and in panel (c) 30-minute averaged TKE are compared at the same stations as in panels (a) and (b) for HS and LS days. All measurements were obtained at 2-m nominal height agl.

3.6 Basin-scale wind patterns

Wind speed during the study period increased with elevation and ERA5-Land modeled wind speed was approximately two times greater than wind speed measured by the benchmark stations at 10-m height (Figure 10). Daily-averaged wind speed for stations over the period of the study were similar on HS versus LS days at elevations ranging from 436 to 1298 m and from

ERA5-Land (Figure 10a), given by close proximity of data markers to the 1-to-1 diagonal. The bars showing ±1 standard deviation for benchmark stations in Figure 10a indicate that variability in measured wind speed was greater for LS days compared to HS days, consistent with subcanopy measurements in WS1 (Figures 7a, 9a). This difference in wind speed variability, however, was not captured by the ERA5-Land analyses. Midday wind direction for all stations (not shown) was upvalley indicating that differential insolation on topography drives basin-scale windflow above the forest canopy for both LS and HS days. On days classified as low-stability, on average, wind speed increased more from 6 AM to the maximum wind speed in the afternoon, both at benchmark stations in canopy gaps and in the ERA-5 reanalysis, compared to high-stability days (Figure 10b). This result indicates that above-canopy mountain breezes accelerated more during LS days. Stronger acceleration of above-canopy winds and increased TKE on LS days relative to HS days moderates solar heating of the canopy and limits development of a within-canopy inversion and down-valley sub-canopy winds (Figure 7).

ERA5-Land pressure gradient and 10-m wind speed provide more support for increased mountain breeze development during LS days. The 00Z (16:00 PST) ERA5-Land surface pressure gradient averaged 2.5% greater on LS days versus HS days for the basin average. Since ERA5-Land gridded products represent averaged quantities for a given grid box, the actual pressure gradient difference over smaller, localized scales likely exceeds this value. An increased horizontal pressure gradient on LS days over the HJ Andrews region favored accelerating above-canopy wind speed and turbulence that would ventilate the canopy, decreasing thermal stratification through the canopy relative to HS days.

Collectively, these results illustrate that low stability days corresponded to days when above-canopy upslope winds directly influenced sub-canopy winds. During days with high in-canopy stability, above canopy winds tended to remain decorrelated from sub-canopy winds throughout the day.

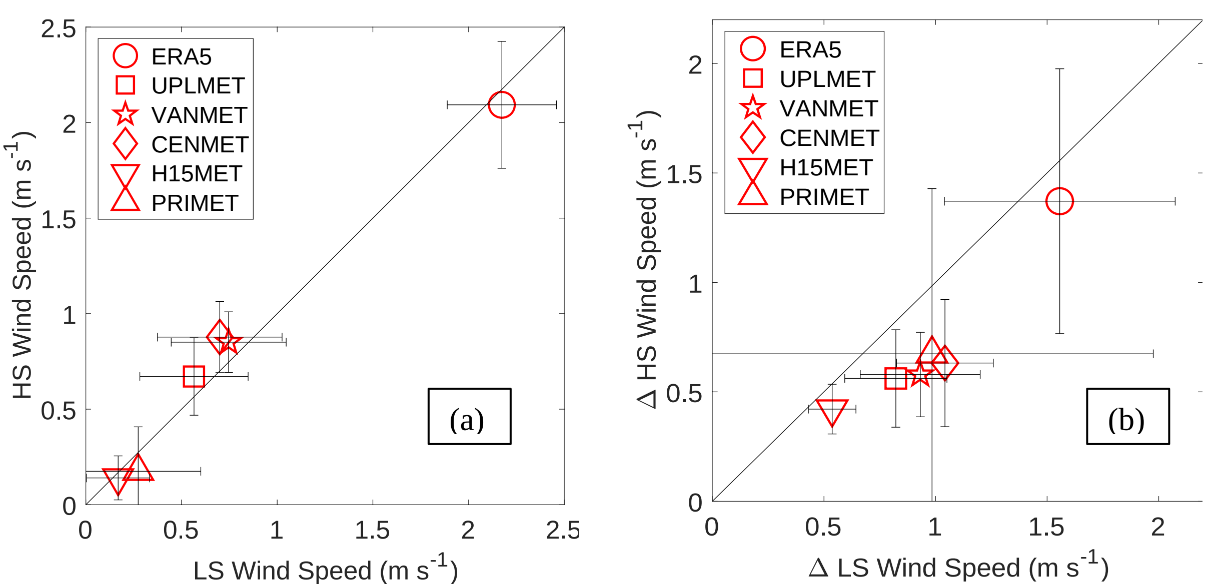

Figure 10. Relationship of average wind speed on high stability days vs. low stability days in the study period (July 19, 2012 to September 17, 2012). (a) Average daily wind speed for HS and LS

days, (b) average daily increase in wind speed from 6AM PST until the afternoon wind speed maximum from ERA5-Land (10-m winds) and at benchmark stations. Vertical and horizontal bars indicate one standard deviation, determined independently for each axis.

3.7 Moisture gradients and fluxes

The difference in daily-composited water vapor concentration between 4 m and 37 m reached its maximum during the DF period on high stability days (Figure 11 a). The gradient of virtual potential temperature, which already accounts for the water vapor influence on buoyancy, was 47% less than the potential temperature gradient between 4 m and 37 m agl at the WS1 tower. So greater sub-canopy moisture decreased within-canopy static stability but not enough to erode the stable layer. Because total precipitation was low (31 mm) and infrequent (spread over 3 days) during the study period (Figure 8), short term differences in vadose zone water available for evaporation or transpiration between HS and LS days were unlikely to account for the observed difference in water vapor concentrations above and below the canopy.

The difference in water vapor concentration between the generally moister sub-canopy and drier above-canopy air increased with sub-canopy static stability (Figure 11b; R^2=0.67). In other words, stronger within-canopy inversions are associated with greater sub-canopy humidity, relative to the air above the canopy. Lower latent heat flux on HS days relative to LS days both above and below the canopy (Fig 7c) as well as lower sub-canopy TKE imply that stronger within-canopy inversions on HS days constrain within-canopy mixing and vertical moisture flux out of the canopy. As vertical mixing is more constrained, subcanopy moisture concentration increases and, for a given downslope wind speed, more moisture is advected downslope by subcanopy winds.

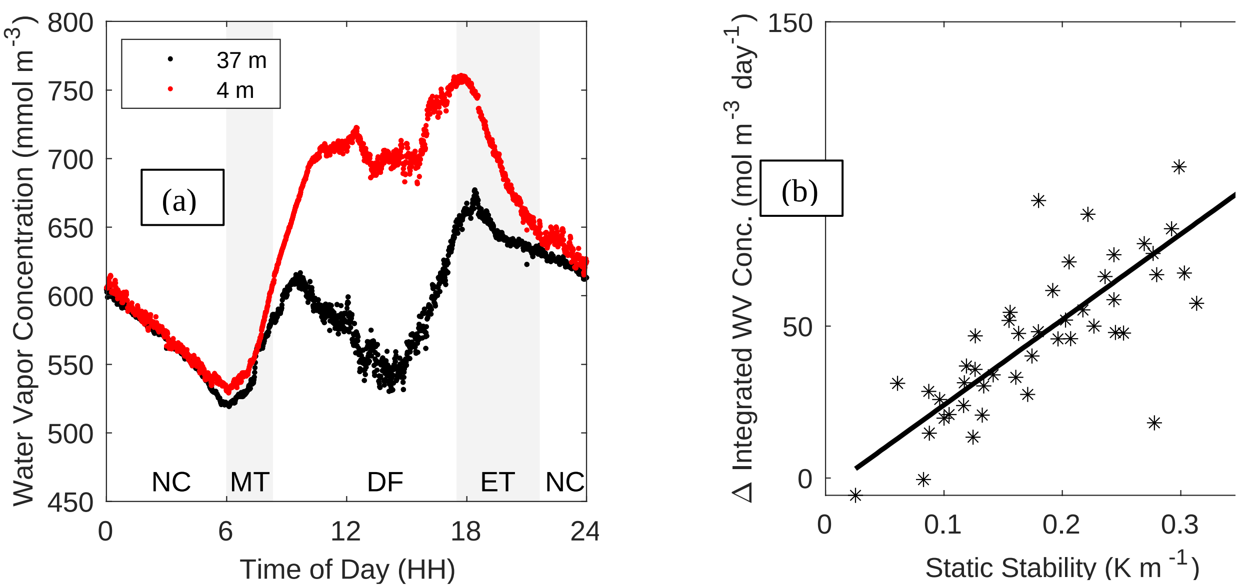

Figure 11. Relationship of water vapor concentration to static stability. (a) Composited water vapor concentration over time during the day for high stability days at 4 m (red) and 37 m

(black). (b) Difference in average daily water vapor concentration, 4 m minus 37 m, versus the daily maximum stability (1 hr averaged) for all days in the study period.

3.8 Wind speed and potential temperature along the watershed axis

The difference in sub-canopy wind speed was positively related to the difference in air temperature between the two along-channel stations (B4 and C4) for HS days in the 50-day IOP (R^2=0.47). The slope of the relationship suggests that a 1 m s^{-1} increase in wind speed corresponds to a 3 °C increase in T_v between these two stations. An increase of 0.1 K m^{-1} in static stability for the 12:30-13:30h period on high stability days is associated with a 0.3 m s^{-1} increase in wind speed (Figure 7a), which in turn corresponds with a 1K increase T_v between B4 and C4, well within the range measured during this experiment. Since sub-canopy wind speed (Figure 7a) and water vapor concentration (Figure 11b) both increase with increasing stability, an increase in static stability produces a positive feedback of water vapor advection through the subcanopy space. For example, for a 0.1 K m^{-1} increase in dry static stability produces a 17% diagnosed increase in water vapor transport by downslope winds relative to the observations (see also the supplement, Section S5).

4 Discussion

The presented results document a flow regime within a PNW coniferous forest that adjusts to the relative intensity of within-canopy static stability. Wind above the canopy can more easily mix with subcanopy air on days when within-canopy stability is low, thereby producing larger latent heat fluxes through the canopy than on days when within-canopy stability is greater. In contrast, strong within-canopy stability restrains vertical moisture flux and engenders increased subcanopy humidity and increased downslope moisture advection. To the authors' knowledge, these linkages between within-canopy stability and vertical vs. downslope vapor transport are a novel finding for forested regions. A linear cause and effect paradigm does not fully describe the development of LS vs. HS days because, for example, greater through-canopy mixing weakens stability, which further promotes vertical moisture flux, reinforcing an LS condition. On HS days, increased downslope moisture advection in a plantation forest changes the distribution of moisture relative to convective mixing. These findings may provide a mechanism to explain observed higher summer evapotranspiration in conifer plantations reported by Perry and Jones (2017), Gronsdahl et al. (2019) and Segura et al. (2020).

Comparing the results of this study with previous studies, the strongest subcanopy downslope winds occurred under the highest stability conditions. However, Wang et al. (2015) found the strongest down-valley winds during moderate stability regimes in a temperate, deciduous forest valley (Wang et al., 2015). Differences in slope and forest canopy structure in this study likely account for different findings compared to Wang et al. (2015). For example, Moon et al. (2019) and Thomas (2011) found large variability in subcanopy wind speed profiles and other statistics caused by variations in canopy structure. Valley configuration (width and depth) also affects the strength of downslope flow and resulting development of a cold air pool (Kiefer & Zhong, 2015). In unvegetated mountains, under high-pressure conditions typical of summer in the Pacific Northwest of the US, local winds convey heat and water vapor upslope during the day, but downslope at night (e.g. Oke, 2002; Geiger, 2009). However, results of this study show that under high pressure conditions, the presence of a forest canopy creates a within-canopy inversion, which strengthens the buoyancy force that drives flow down the slope and enables downslope winds to persist for much of the daytime. TKE and latent heat flux profiles for LS days (Fig 7b) are indicative of above-canopy coherent structures that disturb the sub-canopy air space and promote the loss of sub-canopy moisture by the ejection-sweep process (Finnigan, 1979; Shaw et al., 1983; Thomas et al., 2008).

When considering broader implications of the observations detailed in this study we acknowledge that regional climate models (RCMs) do not resolve the subcanopy wind regime. However, RCMs have skill to predict how climate forcings may change under different climate scenarios and thereby influence sub-canopy moisture transport processes. Regional climate model (~25-km resolution) runs under Representative Concentration Pathway (RCP) 4.5 project an increasing summer/autumn 500 mb high pressure anomaly in the Pacific Northwest (PNW) relative to areas outside of the western US (Rupp et al., 2017). Summer precipitation has been declining since 1980 based on USHCN records for Oregon and Washington (Menne et al., 2009), and is expected to continue to decrease (Rupp et al., 2017). These trends will increase air temperature and vapor pressure and reduce relative humidity above the canopy during the summer, decreasing surface latent heat flux while increasing sensible heat flux from PNW forests. Increases in the ratio of sensible heat flux to latent heat flux (Bowen ratio) increase the strength of mountain breezes (Alpert & Mandel, 1986; De Ridder & Gallée, 1998). Therefore, the increased sensible heat flux over PNW forests predicted by Rupp et al. (2017) would be due not only to energy repartitioning from latent to sensible heat (which is resolvable by an RCM) but also due to increased within-canopy mixing as a consequence of increased surface layer wind speed (which is not resolvable by an RCM). This finding implies that regional climate warming over PNW forests will reduce sub-canopy moisture, potentially limiting moisture-mediated microclimate refugia in these seasonally dry conifer forests (e.g., Davis et al., 2019).

Treating sensible heat flux as an independent variable, increased diabatic heating on a PNW coniferous forest should increase the strength of the mountain breeze on LS days. However, interdependencies of environmental variables and feedbacks between them are not fully understood so we also consider the possibility that winds at canopy level weaken, allowing a strengthened within-canopy inversion. The physical rationale for considering this alternative is that regionally predicted lower relative humidity may increase partitioning of solar insolation into sensible heat, leading to increased warming at canopy level and thereby strengthening the within-canopy inversion on days when above canopy winds do not increase. One can diagnose the increase in wind speed and water vapor concentration as static stability increases on HS days from the slope of the regression that relates wind speed to dry static stability on HS days (Figure 7a) and the slope of the regression that relates water vapor concentration to dry static stability (Figure 11b). Combining these equations allows one to estimate the increase in downslope water vapor transport as static stability increases on HS days. In summary, RCM trends support increasing latent heat flux through the forest canopy on days with low within-canopy stability and increasing downslope advective flux on days with high within-canopy stability.

5 Conclusions

In this intensive field study in a 45-yr-old conifer plantation in a steep mountain valley in Oregon, USA, heating of the forest canopy produced within-canopy inversions, whose strength regulated a bi-modal sub-canopy wind regime during the dry season. On days with relatively weak canopy heating and within-canopy temperature inversions, above canopy winds more efficiently mix subcanopy air, leading to greater than average vertical moisture flux and weaker than average along-slope, sub-canopy water vapor advection. On days with relatively strong canopy heating and within-canopy temperature inversion, vertical moisture flux is suppressed and daytime downslope winds are stronger than average under the canopy.

Increased downslope advection redistributes sub-canopy water vapor and other atmospheric constituents from upslope to downslope areas, providing an alternate method of drying the sub-canopy environment that is not resolved in regional models. Regional-scale increases in Bowen ratio predicted by a regional climate model suggest that both vertical and horizontal water vapor transport from the forest will be enhanced as the climate warms. These findings have implications for how plantation forests respond to climate change.

Future work shall include determining how forest stand structure and landscape patterns interact with wind regimes and climate fluctuations. Building on the methods in this study, further work is needed to resolve spatially distributed pressure gradients and air parcel trajectories into and out of forested mountain valleys to enhance understanding of sub-canopy wind regimes.

Acknowledgments, Samples, and Data

The authors declare that they have no conflict of interest with other affiliations. Funding: this study was supported by NSF Award #0955444 (PI: CKT); funding to the HJ Andrews Forest Long-Term Ecological Research (LTER) program (NSF 1440409, NSF 0823380) and U.S. Forest Service Pacific Northwest Research Station support of hydrology and climate records at the H.J. Andrews Experimental Forest. PI HJO acknowledges partial support by NSF Physical and Dynamic Meteorology (PDM) Grant No. 1848019. SAD acknowledges partial support in the form of startup funding from the University of Nevada, Reno. Benchmark station data (Daly & McKee, 2019) are available as data set MS001 through the Andrews Data Catalog (http://andlter.forestry.oregonstate.edu/data/catalog/datacatalog.aspx). IOP station data Thomas (2017) are available as data set MV007 through the Andrews Data Catalog.

References

Alpert, P., & Mandel, M. (1986). Wind variability—An indicator for a mesoclimatic change in Israel. *Journal of Applied Meteorology and Climatology*, 25(11), 1568-1576. https://doi.org/10.1175/1520-0450(1986)025<1568:WVIFAM>2.0.CO;2

Argerich, A., Haggerty, R., Johnson, S. L., Wondzell, S. M., Dosch, N., Corson-Rikert, H., Ashkenas, L. R., Pennington, R., & Thomas, C. K. (2016). Comprehensive multiyear carbon budget of a temperate headwater stream. *Journal of Geophysical Research-Biogeosciences*, 121(5), 1306-1315. https://doi.org/10.1002/2015JG003050

Brutsaert, W., & Parlange, M. B. (1992). The unstable surface layer above forest: Regional evaporation and heat flux. *Water Resources Research*, 28(12), pp.3129-3134. https://doi.org/10.1029/92WR01860

Campbell Scientific, Inc. (2015). RM Young Wind Monitor Instruction Manual.

Daly, C., Conklin, D. R., & Unsworth, M. H. (2010). Local atmospheric decoupling in complex topography alters climate change impacts. *International Journal of Climatology*, 30(12), 1857-1864. https://doi.org/10.1002/joc.2007

Daly, C., & McKee, W. (2019). Meteorological data from benchmark stations at the Andrews Experimental Forest, 1957 to present. Corvallis, OR: Long-Term Ecological Research. Forest Science Data Bank. doi:10.6073/pasta/c96875918bb9c86d330a457bf4295cd9

Davis, K. T., Dobrowski, S. Z., Holden, Z. A., Higuera, P. E., & Abatzoglou, J. T. (2019). Microclimatic buffering in forests of the future: the role of local water balance. *Ecography*, 42(1), 1-11. https://doi.org/10.1111/ecog.03836

Davis, R., Yang, Z., Yost, A., Belongie, C., & Cohen, W. (2017). The normal fire environment—Modeling environmental suitability for large forest wildfires using past, present, and future climate normals. *Forest Ecology and Management*, 390, 173-186. https://doi.org/10.1016/j.foreco.2017.01.027

de Frenne, P., Lenoir, J., Luoto, M., Scheffers, B. R., Zellweger, F., Aalto, J., ... & Hylander, K. (2021). Forest microclimates and climate change: Importance, drivers and future research agenda. *Global Change Biology*, 27(11), 2279-2297.

De Ridder, K., & Gallée, H. (1998). Land surface–induced regional climate change in southern Israel. *Journal of Applied Meteorology*, 37(11), 1470-1485. https://doi.org/10.1175/1520-0450(1998)037<1470:LSIRCC>2.0.CO;2

Dobrowski, S. Z. (2011). A climatic basis for microrefugia: the influence of terrain on climate. *Global Change Biology*, 17(2), pp.1022-1035. https://doi.org/10.1111/j.1365-2486.2010.02263.x

Ferrez, J., Davison, A. C., & Rebetez, M. (2011). Extreme temperature analysis under forest cover compared to an open field. *Agricultural and Forest Meteorology*, 151(7), 992-1001. https://doi.org/10.1016/j.agrformet.2011.03.005

Finnigan, J. J. (1979). Turbulence in waving wheat. II. Structure of momentum transfer. *Boundary-Layer Meteorology*, 16(3), 213-236. doi:10.1007/BF03335367

Fredriksen, R. L. (1970). Erosion and sedimentation following road construction and timber harvest on unstable soils in three small western Oregon watersheds. Research Papers. Pacific Northwestern Forest and Range Experiment Station, (PNW-104).

Freundorfer, A., Rehberg, I., Law, B. E., & Thomas, C. (2019). Forest wind regimes and their implications on cross-canopy coupling. *Agricultural and Forest Meteorology*, 279, 107696. https://doi.org/10.1016/j.agrformet.2019.107696

Frey, S. J., Hadley, A. S., Johnson, S. L., Schulze, M., Jones, J. A., & Betts, M. G. (2016). Spatial models reveal the microclimatic buffering capacity of old-growth forests. *Science Advances*, 2(4), e1501392. doi:10.1126/sciadv.1501392

Froelich, N. J., & Schmid, H. P. (2006). Flow Divergence and Density Flows above and below a Deciduous Forest: Part II. Below-Canopy Thermotopographic Flows. *Agricultural and Forest Meteorology*, 138. https://doi.org/10.1016/j.agrformet.2006.03.013

Geiger, R., Aron, R.H. & Todhunter, P. (2009). The climate near the ground. Rowman & Littlefield.

Gronsdahl, S., Moore, R. D., Rosenfeld, J., McCleary, R. & Winkler, R. (2019). Effects of forestry on summertime low flows and physical fish habitat in snowmelt-dominant headwater catchments of the Pacific Northwest. *Hydrological Processes*, 33(25), pp.3152-3168. https://doi.org/10.1002/hyp.13580

Halpern, C. B., & Franklin, J. F. (1990). Physiognomie development of Pseudotsuga forests in relation to initial structure and disturbance intensity. *Journal of Vegetation Science*, 1(4), 475-482. https://doi.org/10.2307/3235781

Hansen, M. C., Potapov, P. V., Moore, R., Hancher, M., Turubanova, S. A., Tyukavina, A., Thau, D., Stehman, S. V., Goetz, S. J., Loveland, T. R. & Kommareddy, A. (2013). High-resolution global maps of 21st-century forest cover change. *Science*, 342(6160), pp.850-853. doi:10.1126/science.1244693

Harr, R. D. (1983). Potential for augmenting water yield through forest practices in Western Washington and Western Oregon 1. *Journal of the American Water Resources Association*, 19(3), 383-393. https://doi.org/10.1111/j.1752-1688.1983.tb04595.x

Hersbach, H., Bell, B., Berrisford, P., Hirahara, S., Horányi, A., Muñoz-Sabater, J., et al. (2020). The ERA5 global reanalysis. *Quarterly Journal of the Royal Meteorological Society*, 146(730), 1999–2049. https://doi.org/10.1002/qj.3803

Hicks, B. J., Beschta, R. L., & Harr, R. D. (1991). Long-term changes in streamflow following logging in Western Oregon and associated fisheries implications 1. *Journal of the American Water Resources Association*, 27(2), 217-226. https://doi.org/10.1111/j.1752-1688.1991.tb03126.x

Holden, Z. A., Swanson, A., Klene, A. E.., Abatzoglou, J. T., Dobrowski, S. Z., Cushman, S. A., Squires, J., Moisen, G. G. and Oyler, J. W. (2016). Development of high-resolution (250 m) historical daily gridded air temperature data using reanalysis and distributed sensor networks for the US Northern Rocky Mountains. *International Journal of Climatology*, *36*(10), pp.3620-3632. https://doi.org/10.1002/joc.4580

Hood, E., Gooseff, M. N., & Johnson, S. L. (2006). Changes in the character of stream water dissolved organic carbon during flushing in three small watersheds, Oregon. *Journal of Geophysical Research-Biogeosciences*, 111(G1). https://doi.org/10.1029/2005JG000082

Hosker, R. P., Jr., Nappo, C. P., Jr., & Hanna, S. R. (1974). Diurnal Variation of the Thermal Structure in a Pine Plantation. *Agricultural Meteorology*, 13, 259–265. https://doi.org/10.1016/0002-1571(74)90053-3

Hughes, L. (2000). Biological consequences of global warming: is the signal already apparent? *Trends in Ecology & Evolution*, 15(2), 56-61. https://doi.org/10.1016/S0169-5347(99)01764-4

Jones, J. A. & Hammond, J. C. (2020). River management response to multi-decade changes in timing of reservoir inflows, Columbia River Basin, USA. *Hydrological Processes*, 34(25), pp.4814-4830. https://doi.org/10.1002/hyp.13910

Juang, J. Y., Katul, G. G., Siqueira, M., Stoy, P. C., Palmroth, S., McCarthy, H. R., Kim, H. S., & Oren, R. (2006). Modeling nighttime ecosystem respiration from measured CO2 concentration and air temperature profiles using inverse methods. *Journal of Geophysical Research-Atmospheres*, 111(D8). https://doi.org/10.1029/2005JD005976

Karlsson, I. M. (2000). Nocturnal air temperature variations between forest and open areas. *Journal of Applied Meteorology*, 39(6), 851-862. https://doi.org/10.1175/1520-0450(2000)039<0851:NATVBF>2.0.CO;2

Kiefer, M. T. & Zhong, S. (2013). The effect of sidewall forest canopies on the formation of cold-air pools: A numerical study. *Journal of Geophysical Research: Atmospheres*, 118(12), pp.5965-5978. https://doi.org/10.1002/jgrd.50509

Kiefer, M. T. & Zhong, S. (2015). The role of forest cover and valley geometry in cold-air pool evolution. *Journal of Geophysical Research: Atmospheres*, 120(17), pp.8693-8711. https://doi.org/10.1002/2014JD022998

Launiainen, S., Vesala, T., Mölder, M., Mammarella, I., Smolander, S., Rannik, Ü., Kolari, P., Hari, P., Lindroth, A. & Katul, G. (2007). Vertical variability and effect of stability on turbulence characteristics down to the floor of a pine forest. *Tellus B*, 59(5), pp.919-936. https://doi.org/10.1111/j.1600-0889.2007.00313.x

Lefsky, M. A., Cohen, W. B., Acker, S. A., Parker, G. G., Spies, T. A., & Harding, D. (1999). Lidar remote sensing of the canopy structure and biophysical properties of Douglas-fir western hemlock forests. *Remote Sensing of Environment*, 70(3), 339-361. https://doi.org/10.1016/S0034-4257(99)00052-8

Lembrechts, J. J. and Lenoir, J. (2020). Microclimatic conditions anywhere at any time! *Global Change Biology*, 26(2), pp.337-339.

Lenoir, J., Hattab, T., & Pierre, G. (2017). Climatic microrefugia under anthropogenic climate change: implications for species redistribution. *Ecography*, 40(2), 253-266. https://doi.org/10.1111/ecog.02788

Leuzinger, S., & Körner, C. (2007). Tree species diversity affects canopy leaf temperatures in a mature temperate forest. *Agricultural and Forest Meteorology*, 146(1-2), 29-37. https://doi.org/10.1016/j.agrformet.2007.05.007

Lundquist, J. D., Pepin, N. and Rochford, C. (2008). Automated algorithm for mapping regions of cold-air pooling in complex terrain. *Journal of Geophysical Research: Atmospheres*, 113(D22). https://doi.org/10.1029/2008JD009879

Menne, M. J., Williams Jr., C. N., & Vose, R. S. (2009). The US Historical Climatology Network monthly temperature data, version 2. *Bulletin of the American Meteorological Society*, 90(7), 993-1008. https://doi.org/10.1175/2008BAMS2613.1

Minder, J. R., Mote, P. W. and Lundquist, J. D. (2010). Surface temperature lapse rates over complex terrain: Lessons from the Cascade Mountains. *Journal of Geophysical Research: Atmospheres*, 115(D14). https://doi.org/10.1029/2009JD013493

Moon, K., Duff, T. J., & Tolhurst, K. G. (2019). Sub-canopy forest winds: understanding wind profiles for fire behaviour simulation. *Fire Safety Journal*, 105, 320-329. https://doi.org/10.1016/j.firesaf.2016.02.005

Moore, G. W., Bond, B. J., Jones, J. A., Phillips, N., & Meinzer, F. C. (2004). Structural and compositional controls on transpiration in 40-and 450-year-old riparian forests in western Oregon, USA. *Tree Physiology*, 24(5), 481-491. https://doi.org/10.1093/treephys/24.5.481

Muñoz-Sabater, J., Dutra, E., Agustí-Panareda, A., Albergel, C., Arduini, G., Balsamo, G., Boussetta, S., Choulga, M., Harrigan, S., Hersbach, H., Martens, B., Miralles, D. G., Piles, M., Rodríguez-Fernández, N. J., Zsoter, E., Buontempo, C., Thépaut, J-N. (2021). ERA5-Land: A state-of-the-art global reanalysis dataset for land applications. Earth System Science Data Discussions. Copernicus GmbH, 1–50. https://doi.org/10.5194/essd-2021-82

Nadeau, D. F., Pardyjak, E. R., Higgins, C. W., et al. (2012). Flow during the evening transition over steep Alpine slopes. *Quarterly Journal of the Royal Meteorological Society*, 139:607–624. https://doi.org/10.1002/qj.1985

Nadeau, D. F., Oldroyd, H. J., Pardyjak E. R., et al. (2018). Field observations of the morning transition over a steep slope in a narrow alpine valley. *Environmental Fluid Mechanics*, 1-22. https://doi.org/10.1007/s10652-018-9582-z

NOAA National Centers for Environmental Information, State of the Climate: Drought for Annual 2012, published online January 2013, retrieved on January 3, 2021, https://www.ncdc.noaa.gov/sotc/drought/201213.

Oke, T. R. (2002). Boundary layer climates. Routledge. (p. 178-179).

Oldroyd, H. J., Pardyjak, E. R., Higgins, C. W., & Parlange, M. B. (2016). Buoyant Turbulent Kinetic Energy Production in Steep-Slope Katabatic Flow. *Boundary-Layer Meteorology*, 161:405–416. https://doi.org/10.1007/s10546-016-0184-3

Perry, T. D., & Jones, J. A. (2017). Summer streamflow deficits from regenerating Douglas-fir forest in the Pacific Northwest, USA. *Ecohydrology*, 10(2), e1790. https://doi.org/10.1002/eco.1790

Pypker, T. G., Unsworth, M. H., Lamb, B., Allwine, E., Edburg, S., Sulzman, E., Mix, A. C. & Bond, B. J. (2007). Cold air drainage in a forested valley: Investigating the feasibility of monitoring ecosystem metabolism. *Agricultural and Forest Meteorology*, 145(3-4), 149-166. https://doi.org/10.1016/j.agrformet.2007.04.016

Raynor, G. S. (1971). Wind and temperature structure in a coniferous forest and a contiguous field. *Forest Science*, 17(3), 351-363. https://doi.org/10.1093/forestscience/17.3.351

Ritchie, M. W., Skinner, C. N., & Hamilton, T. A. (2007). Probability of tree survival after wildfire in an interior pine forest of northern California: effects of thinning and prescribed fire. *Forest Ecology and Management*, 247(1-3), 200-208. https://doi.org/10.1016/j.foreco.2007.04.044

Rupp, D. E., Li, S., Mote, P. W., Shell, K. M., Massey, N., Sparrow, S. N., ... & Allen, M. R. (2017). Seasonal spatial patterns of projected anthropogenic warming in complex terrain: a modeling study of the western US. *Climate Dynamics*, 48(7-8), 2191-2213. doi:10.1007/s00382-016-3200-x

Rupp, D. E., Shafer, S. L., Daly, C., Jones, J. A., & Frey, S. J. (2020). Temperature gradients and inversions in a forested Cascade Range basin: Synoptic-to local-scale Controls. *Journal of Geophysical Research: Atmospheres*, 125(23), e2020JD032686. https://doi.org/10.1029/2020JD032686

Schmidli, J. (2013). Daytime heat transfer processes over mountainous terrain. *Journal of the Atmospheric Sciences*, 70:4041–4066. https://doi.org/10.1175/JAS-D-13-083.1

Segura, C., Bladon, K. D., Hatten, J. A., Jones, J. A., Hale, V. C. and Ice, G. G. (2020). Long-term effects of forest harvesting on summer low flow deficits in the Coast Range of Oregon. *Journal of Hydrology*, 585, p.124749. https://doi.org/10.1016/j.jhydrol.2020.124749

Shaw, R. H., Tavangar, J., & Ward, D. P. (1983). Structure of the Reynolds stress in a canopy layer. *Journal of Climate and Applied Meteorology*, 22(11), 1922-1931. https://doi.org/10.1175/1520-0450(1983)022<1922:SOTRSI>2.0.CO;2

Staebler, R. M., & Fitzjarrald, D. R. (2005). Measuring canopy structure and the kinematics of subcanopy flows in two forests. *Journal of Applied Meteorology*, 44(8), 1161-1179. https://doi.org/10.1175/JAM2265.1

Stull, R. B. *An Introduction to Boundary Layer Meteorology* (Vol. 13). Springer Science & Business Media, 2012.

Thomas, C., & Foken, T. (2007). Flux contribution of coherent structures and its implications for the exchange of energy and matter in a tall spruce canopy. *Boundary-Layer Meteorology*, 123(2), 317-337. https://doi.org/10.1007/s10546-006-9144-7

Thomas, C., Martin, J. G., Goeckede, M., Siqueira, M. B., Foken, T., Law, B. E., ... & Katul, G. (2008). Estimating daytime sub-canopy respiration from conditional sampling methods applied to multi-scalar high frequency turbulence time series. *Agricultural and Forest Meteorology*, 148(8-9), 1210-1229. https://doi.org/10.1016/j.agrformet.2008.03.002

Thomas, C. K. (2011). Variability of sub-canopy flow, temperature, and horizontal advection in moderately complex terrain. *Boundary-Layer Meteorology*, *139*(1), 61-81. https://doi.org/10.1007/s10546-010-9578-9

Thomas, C. K., & Smoot, A. R. (2013). An effective, economic, aspirated radiation shield for air temperature observations and its spatial gradients. *Journal of Atmospheric and Oceanic Technology*, 30(3), 526-537. https://doi.org/10.1175/JTECH-D-12-00044.1

Thomas, C. K., Martin, J. G., Law, B. E., & Davis, K. (2013). Toward biologically meaningful net carbon exchange estimates for tall, dense canopies: multi-level eddy covariance observations and canopy coupling regimes in a mature Douglas-fir forest in Oregon. *Agricultural and Forest Meteorology*, 173, 14-27. https://doi.org/10.1016/j.agrformet.2013.01.001

Thomas, C. (2017), Advanced Resolution Canopy FLOw (ARCFLO) experiment employing the SUbcanopy Sonic Anemometer Network (SUSAN) in WS01 of the HJ Andrews Experimental Forest, July-September 2012. Long-Term Ecological Research. Forest Science Data Bank, Corvallis, OR. doi:10.6073/pasta/e1dcac713961e62c3aaad2816bbf7780

Tóta, J., Roy Fitzjarrald, D., & da Silva Dias, M. A. (2012). Amazon rainforest exchange of carbon and sub-canopy air flow: Manaus LBA site—A complex terrain condition. *The Scientific World Journal 2012*. https://doi.org/10.1100/2012/165067

Vickers, D., & Thomas, C. K. (2013). Some aspects of the turbulence kinetic energy and fluxes above and beneath a tall open pine forest canopy. *Agricultural and Forest Meteorology*, 181, 143–151. https://doi.org/10.1016/j.agrformet.2013.07.014

Vickers, D., & Thomas, C. K. (2014). Observations of the scale-dependent turbulence and evaluation of the flux–gradient relationship for sensible heat for a closed Douglas-fir canopy in very weak wind conditions. *Atmospheric Chemistry and Physics*, 14(18), 9665–9676. https://doi.org/10.5194/acp-14-9665-2014

Wang, X., Wang, C., & Li, Q. (2015). Wind regimes above and below a temperate deciduous forest canopy in complex terrain: Interactions between slope and valley winds. *Atmosphere*, 6(1), 60-87. https://doi.org/10.3390/atmos6010060

Whiteman, C. D. (1982). Breakup of temperature inversions in deep mountain valleys: Part I. Observations. *Journal of Applied Meteorology*, 21(3), 270-289. https://doi.org/10.1175/1520-0450(1982)021<0270:BOTIID>2.0.CO;2

Whiteman, C. D. (1990). Observations of thermally developed wind systems in mountainous terrain. In Atmospheric processes over complex terrain (pp. 5-42). *American Meteorological Society*, Boston, MA. https://doi.org/10.1007/978-1-935704-25-6_2

Journal of Geophysical Research: Atmospheres

Supporting Information for

Increasing Daytime Stability Enhances Downslope Moisture Transport in the Subcanopy of an Even-aged Conifer Forest in Western Oregon, USA

S. A. Drake[1,2], D. E. Rupp[2,3], C. K. Thomas[2,4], H. J. Oldroyd[5], M. Schulze,[6] J. A. Jones[2]

[1]Department of Physics, University of Nevada, Reno, Reno, Nevada, 89557, USA.

[2]College of Earth, Ocean, and Atmospheric Sciences, Oregon State University, Corvallis, Oregon, 97331, USA.

[3]Oregon Climate Change Research Institute, College of Earth, Ocean, and Atmospheric Sciences, Oregon State University, Corvallis, Oregon, 97331, USA.

[4]Micrometeorology, University of Bayreuth, Bayreuth, Germany.

[5]Department of Civil and Environmental Engineering, University of California, Davis, Davis, California, 95616, USA.

[6]College of Forestry, Oregon State University, Corvallis, Oregon, 97331, USA.

Contents of this file

Introduction

The following supporting figures and descriptions provide detailed information on findings that are peripheral yet relevant to the main thrust of the manuscript. The drought conditions for June and September 2012 are discussed in Section S1. Section S2 shows the prevailing wind direction at Salem OR, which is NW of the HJ Andrews Experimental Forest during the experiment time frame. Sections S3 and S4 show 1-minute averages of daily pressure (S3) and short-wave insolation (S4) for low and high stability days. Section S5 pictorially represents data discussed in Section 3.8 of the manuscript.

S1. Drought conditions, June and September, 2012

Figure S1a shows the Palmer Z index, a measure of drought conditions, for the continental United States in June 2012. During this period the HJA region had very moist conditions. By September 2012 (Figure S1b) the HJA region was in severe drought conditions.

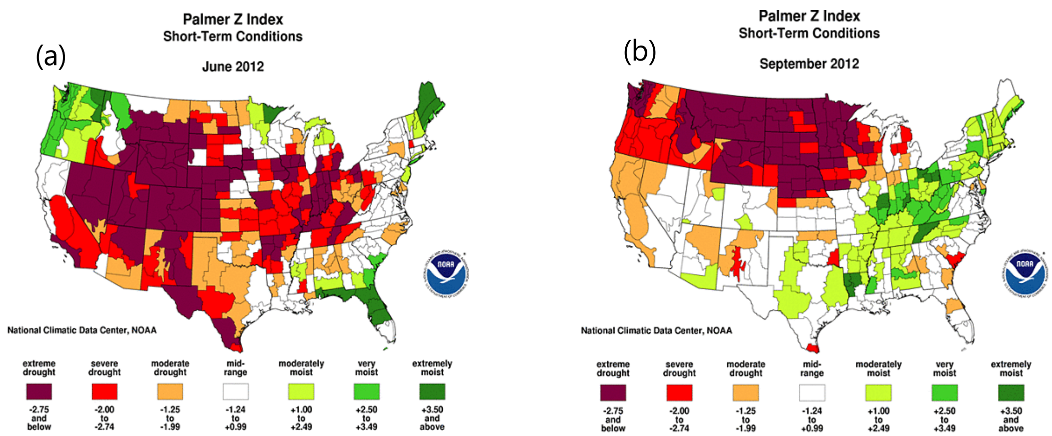

Figure S1. Palmer Z index for June 2012 (panel a) and September 2012 (panel b) for the continental US (Source NOAA NCDC).

S2. Prevailing synoptic wind direction

Figures S2 (a and b) are windroses based on 850 hPa (panel a) and 500 hPa (panel b) rawinsonde winds measured at 00Z by the Salem, Oregon (SLE) NWS office for the time period between July 19 and September 17, 2012, inclusive (data source: http://weather.uwyo.edu/). The Salem site is located approximately 104 km NW of WS1 at the HJ Andrews Experimental Forest. Mid-tropospheric winds are primarily southwesterly during this time period, which was an uncommon wind direction measured at the WS1 tower. These results in comparison with Figure 3 in the manuscript indicate that wind direction measured above and below the canopy at WS1 was due to near-field topographic airflow channeling and basin scale processes rather than synoptic forcing in addition to surface friction in the atmospheric boundary layer.

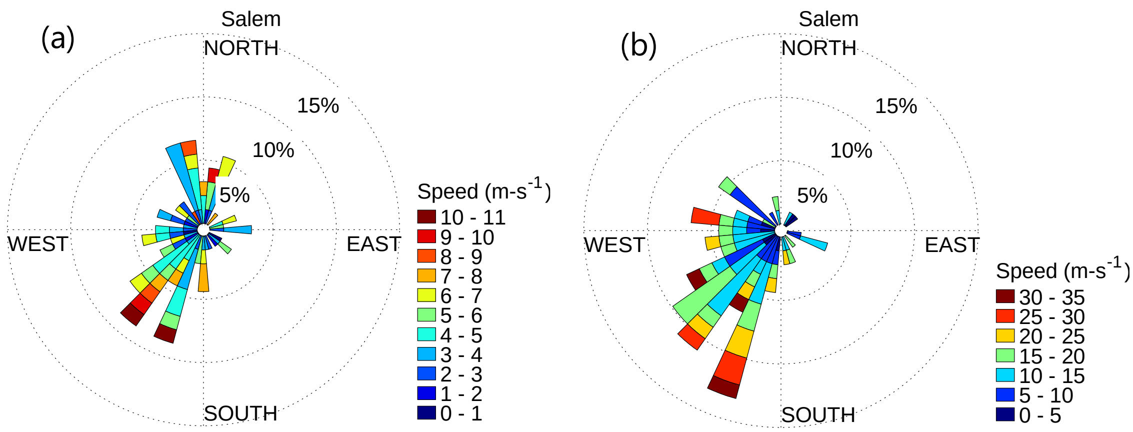

Figure S2. Windrose for 850 hPa (panel a) and 500 hPa level (panel b) derived from 00Z rawinsonde data at Salem Oregon. Timeframe for wind average is between July 19 and September 17, 2012, inclusive.

S3. Daily surface pressure range

Figure S3 shows 1-minute averaged pressure timeseries at the WS1 tower for low stability days (LS, panel a) and high stability days (HS, panel b). In both panels, the ensemble average pressure is displayed as a black line. The systematic afternoon pressure drop had greater amplitude and more coherent timing on HS days than LS days. Coherence in the pressure evolution on HS days suggests sub-canopy breeze development during a time period having a steady-state or systematically consistent pressure gradient evolution at larger-than-watershed scale. The average pressure difference between low stability (LS) and high stability (HS) days was less than 1 hPa as determined for times between 0-6 AM PST. The 0-6 AM PST time range excludes afternoon pressures, which bias HS average pressures downwards due to their larger afternoon pressure decrease. Daily standard deviations were also similar with HS days having a standard deviation of 1.6 hPa and LS days having a standard deviation of 1.2 hPa at WS1. It is important to note that plots in Figure S3 are of the pressure tendency at the WS1 tower, not the (spatial) pressure gradient.

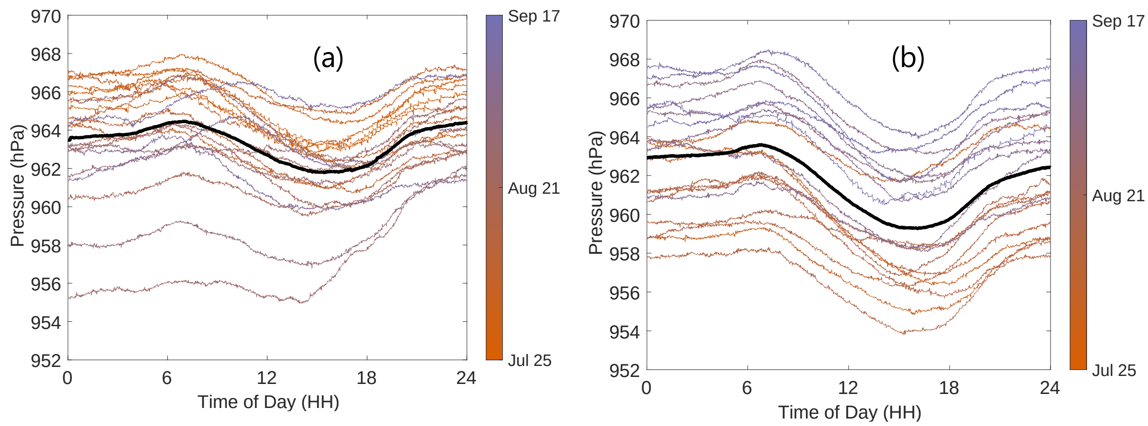

Figure S3. Daily timeseries of air pressure for LS days (panel a) and HS days (panel b) measured at the WS1 tower, color-coded by date. The black line is the ensemble average.

S4. Daily shortwave insolation

Figure S4 shows 1-minute averaged downwelling shortwave radiation measured by a pyranometer mounted at the top of the WS1 tower. Daily integrated downwelling insolation was 2% greater on LS vs. HS days or 11% greater on LS days vs. HS days when excluding overcast and partially overcast days. Although average integrated solar insolation on HS days was lower relative to LS days, HS days were consistently cloud-free or nearly so. These results suggest that the combination of weak synoptic forcing and cloudless days maximized the likelihood of canopy heating and through-canopy stability development.

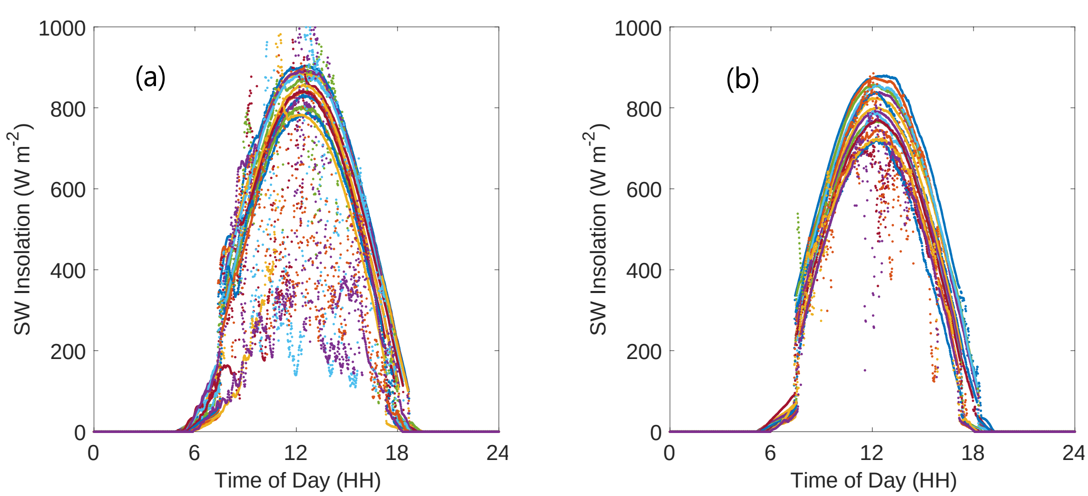

Figure S4. SW insolation for LS days (panel a) and HS days (panel b). Anomalous measurements on Aug 6 and 10, 2012 are not rendered.

S5. Sensitivity of subcanopy transport to downslope temperature gradient

Section 3.7 references a relationship between subcanopy wind speed increase as a function of the temperature difference between stations B4 and C4. Figure 5a shows this relationship. The estimated increase in downslope transport due to increasing subcanopy winds is shown in Fig 5b.

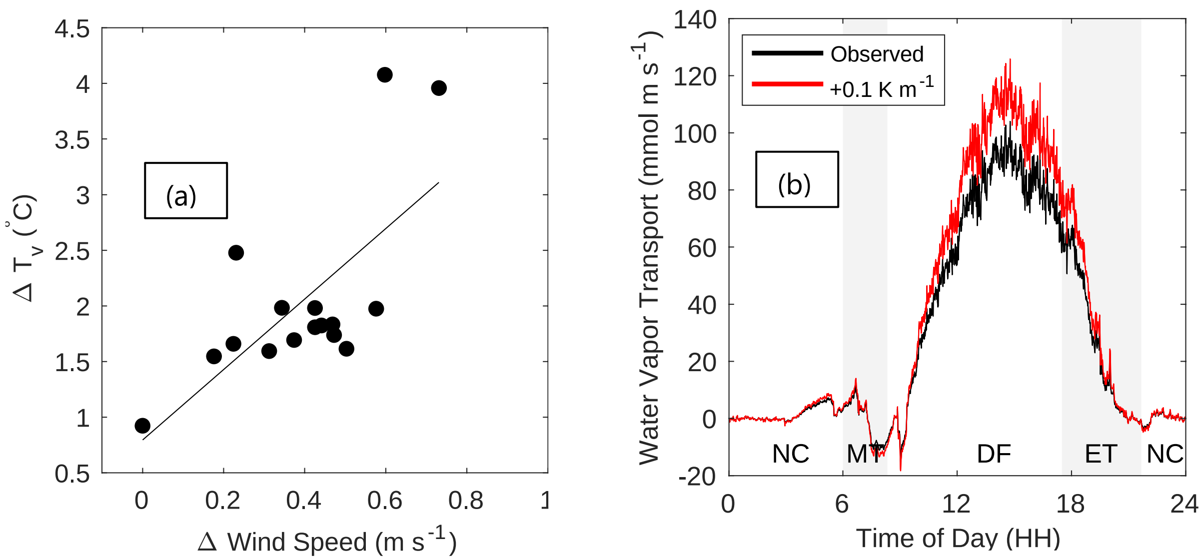

Figure S5. (a) Relationship of differences in wind speed and virtual temperature between stations B4 and C4 for HS days. (b) Composite observed water vapor transport during HS days (black) and the estimated increase in water vapor transport assuming a 0.1 K-m^{-1} static stability increase (red) due to regional climate change.